

Method of simulating hybrid STT-MTJ/CMOS circuits based on MATLAB/Simulink

Min-Hui Ji(冀敏慧) , Xin-Miao Zhang(张欣苗) , Meng-Chun Pan(潘孟春) , Qing-Fa Du(杜青法) , Yue-Guo Hu(胡悦国) , Jia-Fei Hu(胡佳飞) , Wei-Cheng Qiu(邱伟成) , Jun-Ping Peng(彭俊平) , Zhu Lin(林珠) , and Pei-Sen Li(李裴森) ,

Citation: Chin. Phys. B, 2023, 32 (**7**): 078506. DOI: 10.1088/1674-1056/acad69
Journal homepage: http://cpb.iphy.ac.cn; http://iopscience.iop.org/cpb

What follows is a list of articles you may be interested in

Spin transport in epitaxial Fe_3O_4/GaAs lateral structured devices

Zhaocong Huang(黄兆聪), Wenqing Liu(刘文卿), Jian Liang(梁健), Qingjie Guo(郭庆杰), Ya Zhai(翟亚), and Yongbing Xu(徐永兵)

Chin. Phys. B, 2022, 31 (**6**): 068505. DOI: 10.1088/1674-1056/ac4903

The 50 nm-thick yttrium iron garnet films with perpendicular magnetic anisotropy

Shuyao Chen(陈姝瑶), Yunfei Xie(谢云飞), Yucong Yang(杨玉聪), Dong Gao(高栋), Donghua Liu(刘冬华), Lin Qin(秦林), Wei Yan(严巍), Bi Tan(谭碧), Qiuli Chen(陈秋丽), Tao Gong(龚涛), En Li(李恩), Lei Bi(毕磊), Tao Liu(刘涛), and Longjiang Deng(邓龙江)

Chin. Phys. B, 2022, 31 (**4**): 048503. DOI: 10.1088/1674-1056/ac4cc4

Magnetoresistance effect in vertical NiFe/graphene/NiFe junctions

Pei-Sen Li(李裴森), Jun-Ping Peng(彭俊平), Yue-Guo Hu(胡悦国), Yan-Rui Guo(郭颜瑞), Wei-Cheng Qiu(邱伟成), Rui-Nan Wu(吴瑞楠), Meng-Chun Pan(潘孟春), Jia-Fei Hu(胡佳飞), Di-Xiang Chen(陈棣湘), and Qi Zhang(张琦)

Chin. Phys. B, 2022, 31 (**3**): 038502. DOI: 10.1088/1674-1056/ac192e

Magnetic two-dimensional van der Waals materials forspintronic devices

Yu Zhang(张雨), Hongjun Xu(许洪军), Jiafeng Feng(丰家峰), Hao Wu(吴昊), Guoqiang Yu(于国强), and Xiufeng Han(韩秀峰)

Chin. Phys. B, 2021, 30 (**11**): 118504. DOI: 10.1088/1674-1056/ac2808

A novel superjunction MOSFET with improved ruggedness under unclamped inductive switching

Ren Min(任敏), Li Ze-Hong(李泽宏), Deng Guang-Min(邓光敏), Zhang Ling-Xia(张灵霞), Zhang Meng(张蒙), Liu Xiao-Long(刘小龙), Xie Jia-Xiong(谢加雄), and Zhang Bo(张波)

Chin. Phys. B, 2012, 21 (**4**): 048502. DOI: 10.1088/1674-1056/21/4/048502

Method of simulating hybrid STT-MTJ/CMOS circuits based on MATLAB/Simulink

Min-Hui Ji(冀敏慧)[1], Xin-Miao Zhang(张欣苗)[1], Meng-Chun Pan(潘孟春)[1], Qing-Fa Du(杜青法)[1], Yue-Guo Hu(胡悦国)[1], Jia-Fei Hu(胡佳飞)[1], Wei-Cheng Qiu(邱伟成)[1], Jun-Ping Peng(彭俊平)[1], Zhu Lin(林珠)[2], and Pei-Sen Li(李裴森)[1,†]

[1] *College of Intelligence Science and Technology, National University of Defense Technology, Changsha* 410073, *China*
[2] *Beijing National Research Center for Information Science and Technology, Tsinghua University, Beijing* 100084, *China*

(Received 25 October 2022; revised manuscript received 16 December 2022; accepted manuscript online 21 December 2022)

The spin-transfer-torque (STT) magnetic tunneling junction (MTJ) device is one of the prominent candidates for spintronic logic circuit and neuromorphic computing. Therefore, building a simulation framework of hybrid STT-MTJ/CMOS (complementary metal–oxide–semiconductor) circuits is of great value for designing a new kind of computing paradigm based on the spintronic devices. In this work, we develop a simulation framework of hybrid STT-MTJ/CMOS circuits based on MATLAB/Simulink, which is mainly composed of a physics-based STT-MTJ model, a controlled resistor, and a current sensor. In the proposed framework, the STT-MTJ model, based on the Landau–Lifshitz–Gilbert–Slonczewsk (LLGS) equation, is implemented using the MATLAB script. The proposed simulation framework is modularized design, with the advantage of simple-to-use and easy-to-expand. To prove the effectiveness of the proposed framework, the STT-MTJ model is benchmarked with experimental results. Furthermore, the pre-charge sense amplifier (PCSA) circuit consisting of two STT-MTJ devices is validated and the electrical coupling of two spin-torque oscillators is simulated. The results demonstrate the effectiveness of our simulation framework.

Keywords: magnetic tunneling junction (MTJ) model, spin-transfer-torque (STT), circuit simulation, MATLAB/Simulink

PACS: 85.75.–d, 75.47.–m,75.70.–i, 75.75.–c **DOI:** 10.1088/1674-1056/acad69

1. Introduction

With the development of big data and internet of things (IoT), the problems of "memory wall" and "energy wall" caused by the von Neumann bottleneck are becoming increasingly prominent. Recently, spintronics has been regarded as one of the most important technologies to break the bottleneck, due to the advantage of non-volatile, low power, high speed, and compatibility with the traditional complementary metal–oxide–semiconductor (CMOS) devices.[1–4] The spin-transfer-torque (STT) magnetic tunneling junction (MTJ) is one of the most important elements of spintronic technology, which can be used as magnetic memory, magnetic sensors, microwave transmitting and receiving devices.[5–9] The unique multiple functions from sensing, processing to communicating, open the way for the design of new types of computing in sensing devices and paradigms.[10] For example, the spin transfer nano-oscillators (STNOs) have been utilized for the development of new neuromorphic devices and computing paradigms.[11–13] And typically, the hybrid STT-MTJ/CMOS circuits need to be considered in the design process to make full use of advantages of MTJ technology and CMOS technology. Hence, a simulation model that captures the quasi-static and dynamic behaviors of STT-MTJ devices and a hybrid simulation framework of STT-MTJ/CMOS is urgently needed.[14]

Up to now, several hybrid STT-MTJ/CMOS models have been proposed, and most of them are programmed with the SPICE-based circuit simulators or Verilog-A compact model.[14–23] In 2012, Zhang *et al*. reported an compact perpendicular magnetic anisotropy (PMA) STT-MTJ model.[15] This model was programmed with the Verilog-A language. The tunnel resistance effect, the STT switching, and the stochastic behaviors were taken into account. Though this model provides an effective strategy for constructing memory and logic chips, it is personalized for the PMA MTJ devices and the precessional motion is discarded, which is one of the most important characteristics for the design of new generation of neuromorphic devices and oscillator-based computing.[24,25] For the simulation of in-plane magnetic anisotropy (IMA) STT-MTJ, in 2012, Yang *et al*. proposed a modified nodal analysis model with identified internal state variables in SPICE-like simulator,[16] which can deal with the dynamic behavior of devices under arbitrary driving condition, however the model parameters are not directly corresponding to the actual device parameters. Therefore, a timely and comprehensive STT-MTJ model is needed, which can easily adapt to different MTJ parameters and process technologies. Hence, In 2013, Panagopoulos *et al*. developed a physics-based SPICE compact hybrid MTJ/CMOS simulator.[17] The model of MTJ is implemented by using the only inbuilt components (voltage-dependent current sources, capacitors, and

†Corresponding author. E-mail: lpsen@nudt.edu.cn

© 2023 Chinese Physical Society and IOP Publishing Ltd

resistors), the dynamic behavior of MTJ was calculated by Kirchhoff's law. This model provides the ability to predict the real magnet dynamic behaviors of IMA device and PMA STT-MTJ device. Similarly, Kazemi *et al.* reported an adaptive compact MTJ model[18] in 2014, which includes not only the STT effect, but also the voltage controlled magnetic anisotropy (VCMA) effect. This model can also be adapted to IMA and PMA MTJ. Both the models can predict devices' performances from material to circuit level. However, the SPICE-based model using the inbuilt components generally consists of many circuit components or electrical nodes, which are relatively complex.

Simulink provides an interactive graphical model environment and covers the most commonly used SPICE compatible models, which enables rapid construction of a simulation model to explore the design concepts from device to system level. Therefore, in this work, we propose an MATLAB/Simulink based framework for simulating hybrid STT-MTJ/CMOS circuits. The proposed model consists of a physics-based macrospin model of the STT-MTJ device, a controlled resistor, and a current sensor. The STT-MTJ model is edited using the MATLAB script, and the output of the script adjusts the resistance of the controlled resistor, while the current flowing through the controlled resistor will be fed back to STT-MTJ device. Benefited from the modular design of Simulink, the model can be easily expanded by creating a new physical module. Compared with the conventional SPICE-based physics hybrid STT-MTJ/CMOS method, the model presented in this paper is simple, very flexible, and easy to comprehend.

The remainder of this paper is organized as follows. In Section 2 the basic theory and key physics are described, and then the simulation framework based on MATLAB/Simulink is discussed. In Section 3 our proposed model is verified by using experiment results, and the simulation results including the hybrid STT-MTJ/CMOS circuit and the coupling of two devices are also shown. Finally, some conclusions are drawn in Section 4.

2. The simulation framework: Theory and key physics

2.1. MTJ construction and basics

MTJ is a magnetic device consisting of an ultra-thin barrier layer and two ferromagnetic (FM) layers: one has a fixed magnetic orientation (fixed layer), whereas the other (free layer) can change its magnetic orientation. The device structure of MTJ is shown in Fig. 1. The magnetization vector of the free layer and fixed layer are indicated by $\boldsymbol{m}_{\rm f}$ and $\boldsymbol{m}_{\rm p}$, respectively. As is well known, the conductance (G) of the MTJ depends on the angle (θ) between the two magnetization vectors, can be calculated from.[9,26]

$$G = G_{\rm P} + \frac{G_{\rm AP} - G_{\rm P}}{2}\left(1 - \cos\theta\right), \tag{1}$$

where $G_{\rm P}$ and $G_{\rm AP}$ are the conductance of the MTJ device when the magnetic orientations of the two ferromagnetic layers are parallel (P) and antiparallel (AP) to each other, respectively. When the free layer is parallel to the fixed layer, the resistance of MTJ is in the minimum ($R_{\rm P} = 1/G_{\rm P}$) state, while the device is in the high resistance state ($R_{\rm AP} = 1/G_{\rm AP}$) when the relative magnetic orientations are antiparallel. The TMR ratio can be represented by the following equation, which decreases with the bias voltage $V_{\rm bias}$ increasing:[27]

$$\mathrm{TMR} = \frac{\mathrm{TMR}\left(0\right)}{\left[1 + \left(V_{\rm bias}/V_{\rm h}\right)^2\right]} = \frac{R_{\rm AP} - R_{\rm P}}{R_{\rm P}}, \tag{2}$$

where TMR is the measured real value, TMR(0) is the TMR value when the bias voltage is close to zero, and $V_{\rm h}$ is the corresponding bias voltage when $\mathrm{TMR} = 0.5 \times \mathrm{TMR}(0)$.

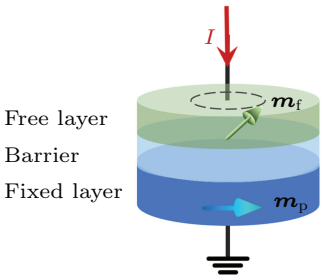


Fig. 1. Basic schematic diagram of MTJ structure consisting of a free layer, a barrier layer, and a fixed layer.

2.2. Theories of magnetization dynamics

The free layer magnetization is macrospin approximately in our model.[28] The magnetization precession motion can be explained by the Landau–Lifshitz–Gilbert (LLG) equation with the additional Slonczewski's term,[16,29,30] and the equation is shown as follows:

$$\begin{aligned}
&\frac{\mathrm{d}\boldsymbol{m}_{\rm f}}{\mathrm{d}t} = -\left|\gamma\right|\boldsymbol{m}_{\rm f}\times\boldsymbol{H}_{\rm eff} + \alpha\boldsymbol{m}_{\rm f}\times\frac{\mathrm{d}\boldsymbol{m}_{\rm f}}{\mathrm{d}t} \\
&\qquad + \left|\gamma\right|\alpha_{\rm J}\boldsymbol{m}_{\rm f}\times\left(\boldsymbol{m}_{\rm f}\times\boldsymbol{m}_{\rm p}\right) - \left|\gamma\right|\beta_{\rm J}\boldsymbol{m}_{\rm f}\times\boldsymbol{m}_{\rm p}, \\
&\beta = \left|\frac{\hbar}{\mu_0 e}\right|\frac{\boldsymbol{J}}{tM_{\rm s}}, \\
&g = \frac{P\Lambda^2}{\left(\Lambda^2+1\right) + \left(\Lambda^2-1\right)\left(\boldsymbol{m}_{\rm f}\cdot\boldsymbol{m}_{\rm p}\right)}, \\
&\alpha_{\rm J} = \beta g, \quad \text{and} \quad \beta_{\rm J} = \beta\varepsilon.
\end{aligned} \tag{3}$$

Here, $\boldsymbol{m}_{\rm f}$ and $\boldsymbol{m}_{\rm p}$ are the reduced magnetization vectors of the free layer and unit polarization direction of fixed layer, respectively, γ is the gyromagnetic ratio, $\boldsymbol{H}_{\rm eff}$ is the effective field, α is the Gilbert damping factor, $\alpha_{\rm J}$ is the STT coefficient, and $\beta_{\rm J}$ is the field-like torque coefficient. In the definition of β, $\boldsymbol{J}$ is the current density, and it is assumed to be uniformly distributed on the surface. In this work, positive $\boldsymbol{J}$ is defined as electrons flowing from the fixed layer to free layer, $\hbar$ is the

reduced Planck constant, μ is the vacuum permeability, e is the electronic charge, M_s is the saturation magnetization, and t is the thickness of the free layer. The polarization function g is dependent on the angle between $\boldsymbol{m}_f$ and $\boldsymbol{m}_p$, P is the spin polarization factor, Λ is the torque asymmetry parameter, and ε is the secondary spin transfer term. The effective field $\boldsymbol{H}_{eff}$ can be expressed as the sum of several different fields, including the applied external magnetic field ($\boldsymbol{H}_{ext}$), the effective uniaxial anisotropy field ($\boldsymbol{H}_k$), the demagnetization field ($\boldsymbol{H}_d$) and the thermal noise field ($\boldsymbol{H}_{th}$)[31] as follows:

$$\boldsymbol{H}_{eff} = \boldsymbol{H}_{ext} + \boldsymbol{H}_k + \boldsymbol{H}_d + \boldsymbol{H}_{th}, \tag{4}$$

$$\boldsymbol{H}_k = \frac{2K_u}{\mu_0 M_s}\left(\boldsymbol{m}_f \cdot \boldsymbol{m}_p\right)\boldsymbol{m}_p, \tag{5}$$

$$\boldsymbol{H}_d = -\left(\boldsymbol{N} \cdot \boldsymbol{m}_f\right)M_s, \tag{6}$$

$$\boldsymbol{H}_{th} = \chi\sqrt{\frac{\alpha}{1+\alpha^2}\frac{2k_B T}{\gamma\mu_0 M_s V \delta_t}}, \tag{7}$$

where K_u is the effective uniaxial anisotropy coefficient; $\boldsymbol{N}$ is the demagnetizing factor, which depends on the shape and size of the free layer;[32] χ is a three-dimensional Gaussian distribution with a zero mean and standard deviation, k_B is the Boltzmann constant, T is the temperature, V is the volume of the computational cell, and δ_t is the simulation time step.

2.3. MATLAB/Simulink implementation

The proposed hybrid simulation framework can be divided into two main modules: the first is the simulation of the physics-based STT-MTJ model and the second is the analysis of the controlled resistance and peripheral circuit as shown in Fig. 2.

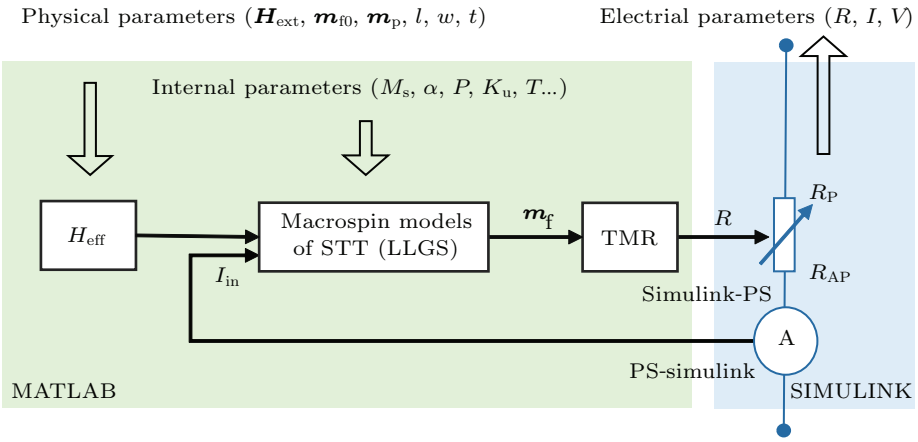


Fig. 2. Proposed hybrid MTJ-STT/CMOS modeling framework.

For the simplicity of simulation hybrid STT-MTJ/CMOS circuit, a MATLAB function block is used and the physics-based STT-MTJ model is edited using the MATLAB script. First, the external magnetic field $\boldsymbol{H}_{ext}$ should be offered, the initial magnetization states of free layer ($\boldsymbol{m}_{f0}$), the fixed layer magnetization vector ($\boldsymbol{m}_p$) and physical size of the device (l: length, w: width, and t: thickness) are input. The magnetic internal parameters mentioned above (M_s, α, P, K_u, T,...) are preset. And the effective field mentioned above (Eqs. (4)–(7)) are considered in the simulation of the physics model. The LLGS equation is solved by using the improved Euler method. Therefore, the free layer magnetization vector ($\boldsymbol{m}_f$) can be obtained and the resistance (R) of the device can be calculated from Eqs. (1)–(3), as shown in the green part of Fig. 2. The calculated resistance value R is converted into a physical signal by using the Simulink-PS converter block. Therefore, the calculated value R that can control the resistance of the physically controlled resistor, changes from R_P to R_{AP}. The electrical ports of the controlled resistor can be connected with other semiconductor devices and electrical sources. Furthermore, the current sensor is used to obtain the current in the electric circuit. Then, the PS-Simulink converter block converts the physical current into the Simulink signal I_{in}, which is used as an input current of the physics-based STT-MTJ model.

3. Simulation results

3.1. Physics-based STT-MTJ model

In this subsection, the proposed physics-based STT-MTJ model is verified with the experimental result. The devices studied here have the following stack bottom electrode/PtMn(15)/$Co_{70}Fe_3$(2.3)/Ru(0.85)/$Co_{40}Fe_{40}B_{20}$(2.4)/MgO(0.8)/$Co_{20}Fe_{60}B_{20}$(2.0)/top electrode (numbers in bracket denotes the thickness in unit nm), and then the stacks are fabricated into pillar shaped device with the cross-section area of 100 nm×120 nm×π/4. The schematic diagram of the STT-MTJ device stacks is illustrated in Fig. 3(a). And the measured typical resistance curve scan as a function of I is shown in Fig. 3(b) (the black curve).

The simulation is conducted by sweeping the current I in steps of δI. And under each current, the LLGS model is solved with a fixed time step of δ_t. After each time step,

the instantaneous resistance $R(t)$ is calculated. Based on this, the time-averaged resistance is used to evaluate the resistance for each I. The red curve shown in Fig. 3(b) represents the device's switching characteristics calculated by using the parameters in the third column of Table 1 (switching behavior simulation values), and the values of $R_{\rm P}$ and $R_{\rm AP}$ are 1 kΩ and 2 kΩ, respectively. The results show that our proposed model can capture the dynamic switching characteristics accurately. Figures 3(c) and 3(d) show the time-domain transient resistance values and the magnetization precession three-dimensional (3D) trajectories of the device at different bias currents. It can be observed that at $I = 0.3$ mA, the resistance is equal to $R_{\rm P}$, and the precession of the free layer is around $\boldsymbol{m}_{\rm p}$. As the current decreases to −0.54 mA, the STT-MTJ switches from $R_{\rm P}$ to $R_{\rm AP}$. The $\boldsymbol{m}_{\rm f}$ precesses around the $\boldsymbol{m}_{\rm p}$ initially, and finally stabilizes in the antiparallel direction. The resistance in antiparallel state is affected by the voltage, and the resistance is about 1800 Ω at $I = 0.06$ mA. As the current reaches 0.08 mA, the resistance drops from $R_{\rm AP}$ to $R_{\rm P}$.

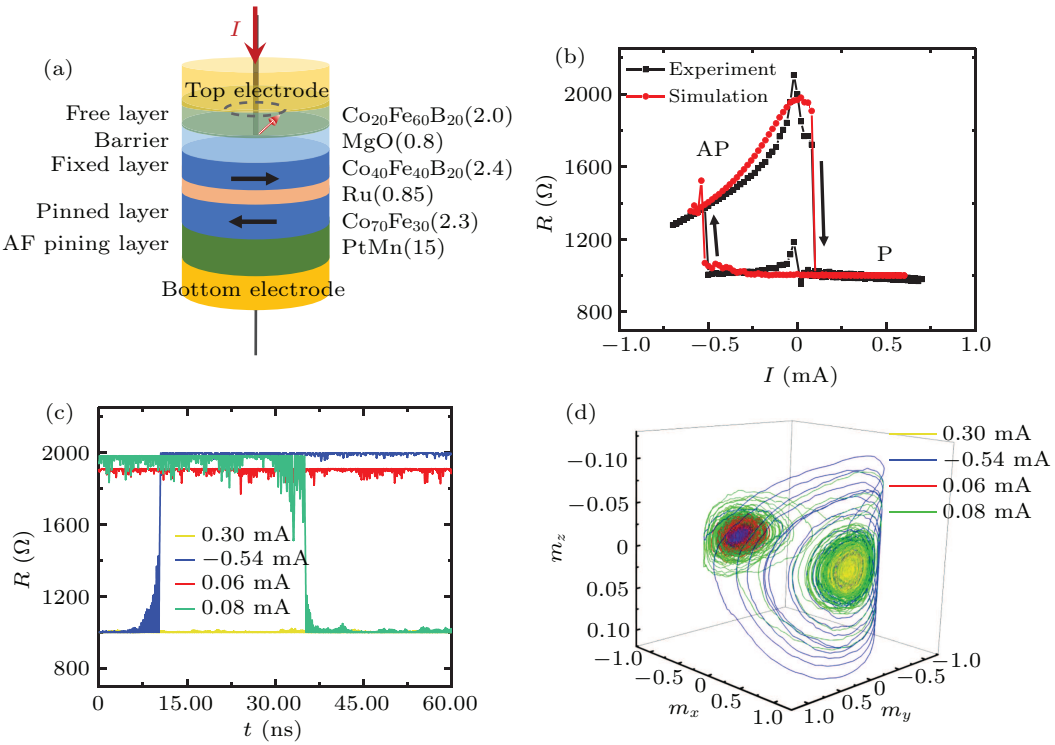


Fig. 3. (a) Schematic illustration of STT-MTJ device, (b) measured and simulated variation of resistance with current of STT-MTJ, with $\boldsymbol{H}_{\rm ext}$ equaling 0 Oe (the unit 1 Oe = 79.5775 A·m^{-1}), (c) time-dependent resistances, and (d) free layer precession 3D trajectories of the STT-MTJ device at different input currents.

Table 1. Parameters for simulating STT-MTJ switching and oscillation behaviors.

Variables	Parameters	Switching behavior simulation values	Oscillation behavior simulation values
l (nm)	free layer length	100	150
w (nm)	free layer width	120	75
t (nm)	free layer thickness	2.0	1.6
$M_{\rm s}$ (A·m^{-1})	saturation magnetization	1060×10^3	1100×10^3
P	spin polarization factor	0.57	0.57
α	Gilbert damping factor	0.008	0.01
T (K)	temperature	300	0 K without noise 300 K with noise
$K_{\rm u}$ (J·m^{-3})	uniaxial anisotropy coefficient	3.4×10^3 in plane	7.2×10^5 out of plane
Λ	torque asymmetry parameter	2.25	2.25
ε	secondary spin transfer parameter	−1	−1
$\delta_{\rm t}$ (s)	simulation time update step	3×10^{-12}	5×10^{-12}
$\boldsymbol{m}_{\rm p}$	direction of fixed layer	$\varphi = 10/180\times\pi$ $(\cos(\varphi), \sin(\varphi), 0)$	$\varphi = 10/180\times\pi$ $(\cos(\varphi), \sin(\varphi), 0)$
TMR(0)	TMR value (bias voltage is zero)	100%	
$V_{\rm h}$	bias voltage	0.6	

The STT-MTJ model used for analyzing the microwave oscillation characteristics is based on the experimental data presented by Zeng *et al.*[33] For the large interfacial perpendicular anisotropy, the stable oscillation can be achieved without an external magnetic field. The parameters used to match the sustained oscillations are listed in the last column in Table 1 (oscillation behavior simulation values) and the interfacial perpendicular anisotropy is included in the effective uniaxial anisotropy. Figure 4(a) shows the time-dependent transient resistance with the input current $I = -0.2$ mA (the total simulation time is 60 ns, to observe the change of resistance clearly, only the results within 10 ns are shown here). Figure 4(b) shows the FFT result of the transient resistance. As can be seen from the figure, the fundamental frequency is 1.01 GHz. The 3D trajectory of the $\boldsymbol{m}_{\rm f}$ magnetization is shown in Fig. 4(c), which is initially circular and gradually evolves into stable out-of-plane precession orbits. Figure 4(d) shows the microwave oscillation fundamental frequency as a function of bias current. The black curve is the experiment result reproduced from Zeng *et al.*'s work,[33] the red circles and blue triangles show the simulation results based on our framework without and with the thermal noise, respectively. Note that the simulation results are consistent with the experimental results, and the oscillation frequency decreases with the increase of absolute current value at a rate of about 1.78 GHz/mA, demonstrating the validity of our proposed physics-based STT-MTJ model.

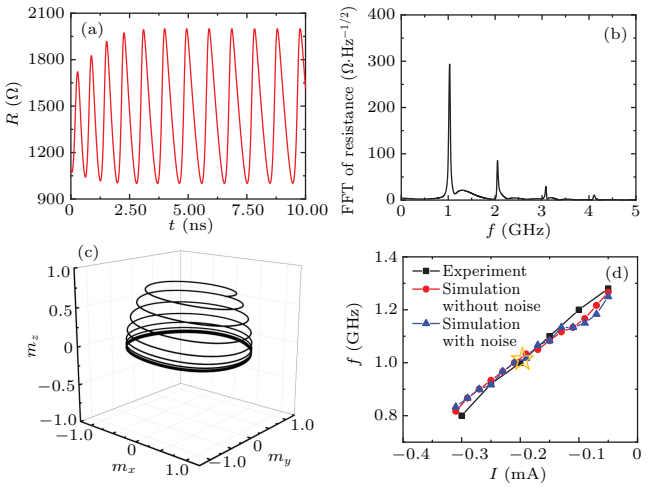


Fig. 4. (a) Resistance, (b) resistance spectrum, and (c) free layer precession 3D trajectory of STNO device when the input current is −0.2 mA. (d) STNO oscillation fundamental frequency as a function of I with and without thermal noise with $\boldsymbol{H}_{\rm ext}$ equaling 0 Oe, the point marked in pentagram indicating that the corresponding frequency is 1.01 GHz when the input current is −0.2 mA.

3.2. Devices level simulation

For the hybrid simulation of STT-MTJ/CMOS circuits, our proposed framework is used to simulate the pre-charge sense amplifier (PCSA) circuit proposed by Zhao *et al.*[34] The circuit is composed of two STT-MTJ devices, three NMOS transistors and four PMOS transistors. The circuit can sense the magnetic configuration of the MTJ at a high speed. Figure 5(a) shows the schematic of the proposed circuits, where $R_{\rm P}$ and $R_{\rm AP}$ of the STT-MTJ device are 4.7 kΩ and 11.7 kΩ, respectively, and the remaining magnetic parameters are the same as the switching behavior simulation values. Moreover the parameters of the transistors are based on the 90-nm BSIM4 model.[35] The control signals and the corresponding simulation results are shown in Fig. 5(b). It is observed that when "SEN" is set to zero, the polarization voltages of the two MTJs, $Q_{\rm m}$ and $Q_{\rm m_bar}$ are both equal to $V_{\rm dd}$. And when "SEN" changes to a high level, both two voltages begin to decrease due to MTJs discharging. The resistance of MTJ1 is set to $R_{\rm AP}$, whereas the resistance of MTJ0 is $R_{\rm P}$. Therefore, the discharge speed in the MTJ0 branch is faster than that in the MTJ1 branch. When the difference between $Q_{\rm m}$ and $Q_{\rm m_bar}$ is less than the threshold voltage of P1, the P1 will be open and $Q_{\rm m_Bar}$ will be charged to $V_{\rm dd}$, while $Q_{\rm m}$ will continue discharge to zero potential. The simulation result is consistent with the result in Ref. [34].

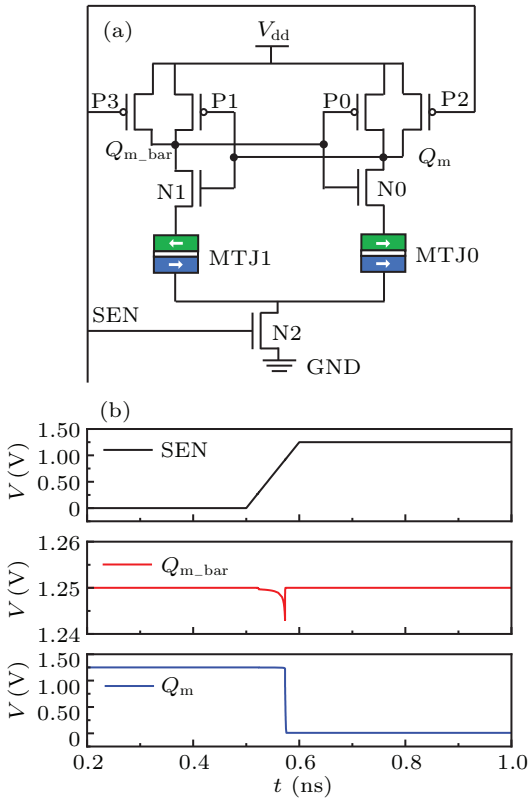


Fig. 5. (a) PCSA circuit consisting of STT-MTJ devices, three NMOS transistors and four PMOS transistors, (b) control single (SEN) and the simulated voltage results of $Q_{\rm m}$ and $Q_{\rm m_bar}$.

The coupling of the STNOs is a promising component for neuromorphic computing and associative memory.[13] And our proposed framework can emulate the coupling characteristics of the STNO conveniently. Figure 6(a) shows the electrical coupling simulation method of two STNOs.[4] The simulation parameters are the same as the ones listed in Table 1 (oscil-

lator behavior simulation values). The independent bias currents ($I_{\rm bias1}$ and $I_{\rm bias2}$) and external magnetic fields ($\boldsymbol{H}_{\rm bias1}$ and $\boldsymbol{H}_{\rm bias2}$) are applied to STNOs. By appropriately controlling the bias current and external magnetic field, the microwave signal can be generated, and the devices are coupled with each other. The $I_{\rm broadcast}$ on the feedback branch is calculated from the following equation:

$$I_{\rm broadcast\ \mathit{i}} = \frac{1}{2}\left(C_1 m_{x1} + C_1 m_{x2}\right), \tag{8}$$

where C_1 and C_2 are the coupling constants, which are determined by the coupling circuit; m_{x1} and m_{x2} are free layer magnetization x-direction components. The currents flowing through the STNO are $I_{\rm input1}$ and $I_{\rm input2}$, respectively. Therefore, the input current is the combination of the bias current and feedback current

$$I_{\rm input\ \mathit{i}} = I_{\rm bias\ \mathit{i}} + I_{\rm broadcast\ \mathit{i}}. \tag{9}$$

Based on the proposed electrical coupling simulation method, in order to analyze the coupling behavior, the bias current and external magnetic field are changed independently. First, the bias currents of both STNOs are kept at -0.2 mA. The external magnetic field, perpendicular to plane free layer, of STNO2 is constant at a zero magnetic field, while the magnetic field sensed by STNO1 changes from -3 mT to 3 mT. For a non-zero coupling coefficient ($C_1 = C_2 = 0.01$), the frequency of the two STNOs is locked in a suitable magnetic field range from -0.6 mT to 0.6 mT. The simulation results are shown in Fig. 6(b). In addition, the external magnetic field of the two STNOs is set to 0 mT, the $I_{\rm bias2}$ is set to -0.2 mA, while the $I_{\rm bias1}$ is varying. The coupling coefficients remain unchanged. The oscillation frequencies of the two STNOs are shown in Fig. 6(c), which demonstrate the same rules as unilaterally changing $\boldsymbol{H}_{\rm bias1}$.

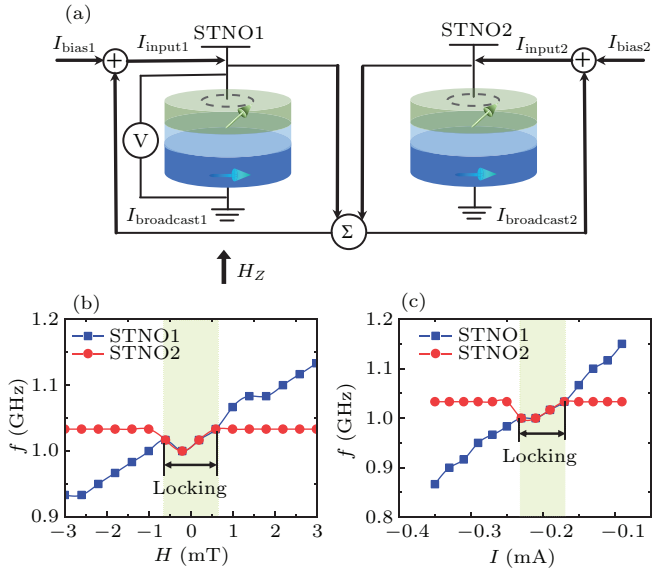


Fig. 6. (a) Schematic diagram of two STNOs with electrical coupling, STNO oscillation frequencies as a function of (b) magnetic field applied perpendicular to the plane of free layer and (c) bias current under constant zero magnetic field ($T = 0$ K).

4. Conclusions

This work presents a hybrid STT-MTJ/CMOS model framework based on MATLAB/Simulink, which is mainly composed of a physics-based STT-MTJ model, a controlled resistor, and a current sensor. The physics model developed under the single domain approximation is benchmarked with experimental results. Based on the proposed hybrid STT-MTJ/CMOS model framework, the PCSA circuit consisting of two STT-MTJ devices and the coupling of two STNOs are simulated. The simulation results are consistent with the published results. It is pointed out that the model is applicable to both IMA device and PMA STT-MTJ device by presetting the direction of fixed layer and uniaxial anisotropy parameter. Our proposed model paves the way for the hybrid STT-MTJ/CMOS simulation of device, circuit, and system architecture, including not only the design of spin-based logic and memory devices, but also the development of the neuromorphic devices and oscillation-based computing framework.

Acknowledgements

Project supported by the National Natural Science Foundation of China (Grant No. 62004223), the Science and Technology Innovation Program of Hunan Province, China (Grant No. 2022RC1094), the Open Research Fund Program of the State Key Laboratory of Low-Dimensional Quantum Physics, China (Grant No. KF202012), and the Hunan Provincial Science Innovation Project for Postgraduate, China (Grant No. CX20210086).

References

[1] Finocchio G, Di Ventra M, Camsari K Y, Everschor-Sitte K, Khalili A P and Zeng Z M 2021 *J. Magn. Magn. Mater.* **521** 167506
[2] Grollier J, Querlioz D and Stiles M D 2016 *Proc. IEEE* **104** 2024
[3] Yogendra K, Fan D, Jung B and Roy K 2016 *IEEE T. Electron Dev.* **63** 1674
[4] Yogendra K, Liyanagedera C, Fan D, Shim Y and Roy K 2017 *ACM J. Emerg. Technol. Comput. Sys.* **13** 56
[5] Apalkov D, Dieny B and Slaughter J M 2016 *Proc. IEEE* **104** 1796
[6] Oh I Y, Park S Y, Kang D H and Park C S 2014 *IEEE Microw. Wirel. Compon. Lett.* **24** 502
[7] Fang B, Carpentieri M, Hao X, Jiang H, Katine J A, Krivorotov I N, Ocker B, Langer J, Wang K L, Zhang B, Azzerboni B, Amiri P K, Finocchio G and Zeng Z M 2016 *Nat. Commun.* **7** 11259
[8] Yin X L, Yang Y, Liu Y F, Hua J, Sokolov A, Ewing D, De R P J, Gao K Z and Liou S H 2019 *Spintronics XII* (San Diego) p. 110903H
[9] Atsufumi H, Keisuke Y, Yoshinobu N, Ioan L P, Bernard D, Philipp P and Burkard H 2020 *J. Magn. Magn. Mater.* **509** 166711
[10] Locatelli N, Cros V and Grollier J 2014 *Nat. Mater.* **13** 11
[11] Mazza L, Puliafito V, Raimondo E, Giordano A, Zeng Z, Carpentieri M and Finocchio G 2022 *Phys. Rev. Appl.* **17** 014045
[12] Sengupta A, Panda P, Wijesinghe P, Kim Y and Roy K 2016 *Sci. Rep.* **6** 30039
[13] Romera M, Talatchian P, Tsunegi S, Yakushiji K, Fukushima A, Kubota H, Yuasa S, Cros V, Bortolotti P, Ernoult M, Querlioz D and Grollier J 2022 *Nat. Commun.* **13** 883
[14] Joshi V K, Barla P, Bhat S and Kaushik B K 2020 *IEEE Access* **8** 194105

[15] Zhang Y, Zhao W S, Lakys Y, Klein J O, Kim J V, Ravelosona D and Chappert C 2012 *IEEE T. Electron Dev.* **59** 819

[16] Yang S, Wei F and Hao Y 2012 17*th Asia and South Pacific Design Automation Conference* 2012, January 30–February 2, Sydney, NSW, Australia, p. 529

[17] Panagopoulos G D, Augustine C and Roy K 2013 *IEEE T. Electron Dev.* **60** 2808

[18] Kazemi M, Ipek E and Friedman E G 2014 *IEEE T. Electron Dev.* **61** 3883

[19] Li Q Y, Zhang P H and Li H T 2021 *Chin. Phys. B* **30** 047504

[20] Hu X T A, Brigner W H, Incorvia J A C and Friedman J S 2019 *IEEE T. Electron Dev.* **66** 2817

[21] Fernando G R, Pranay P, Mudit D and Cyrille D 2021 *SMACD/PRIME* 2021 *International Conference on SMACD and* 16*th Conference on PRIME*, July 19–22 online p. 1

[22] Wang Y, Cai H, Naviner L A B, Zhang Y, Klein J O and Zhao W S 2015 *Microelectron Reliab.* **55** 1649

[23] György C, Matt P, Dmitri E N, George I B, Andras H, Tamas R and Wolfgang P 2012 13*th International Workshop on Cellular Nanoscale Networks and their Applications*, August 29–31, Turin, Italy, p. 1

[24] Csaba G and Porod W 2020 *Phys. Rev. Appl.* **7** 011302

[25] Leroux N, Mizrahi A, Marković1 D, Sanz-Hernández D, Trastoy J, Bortolotti P, Martins L, Jenkins A, Ferreira R and Grollier J 2021 *Neuromorph. Comput. Eng.* **1** 011001

[26] Miwa S, Ishibashi S, Tomita H, Nozaki T, Tamura E, Ando K, Mizuochi N, Saruya T, Kubota H, Yakushiji K, Taniguchi T, Imamura H, Fukushima A, Yuasa S and Suzuki Y 2014 *Nat. Mater.* **13** 50

[27] Zhang S, Levy P M, Marley A C and Parkin S S P 1997 *Phys. Rev. Lett.* **79** 3744

[28] Jiang X, A Zang W and Mark D S 2005 *Phys. Rev. B* **72** 014446

[29] NIST OOMMF userguide, 2018

[30] Slonczewski J C 1996 *J. Magn. Magn. Mater.* **159** L1

[31] Zhang X, Ezawa M, Xiao D, Zhao G. P, Liu Y and Zhou Y 2015 *Nanotechnology* **26** 225701

[32] Osborn J A 1945 *Phys. Rev.* **67** 351

[33] Zeng Z M, Finocchio G, Zhang B, Khalili A P, Katine J A, Krivorotov I N, Huai Y, Langer J, Azzerboni B, Wang K L and Jiang H 2013 *Sci. Rep.* **3** 1426

[34] Zhao W S, Chappert C, Javerliac V and Noziere J P 2009 *IEEE Trans. Magn.* **45** 3784

[35] 90 nm BSIM4 model card for bulk CMOS.